Volume-Preserving Nonrigid Registration of MR Breast Images Using Free-Form Deformation With an Incompressibility Constraint

Torsten Rohlfing, Calvin R. Maurer, Jr.*, *Member, IEEE,* David A. Bluemke, and Michael A. Jacobs

***Abstract*—In this paper, we extend a previously reported intensity-based nonrigid registration algorithm by using a novel regularization term to constrain the deformation. Global motion is modeled by a rigid transformation while local motion is described by a free-form deformation based on B-splines. An information theoretic measure, normalized mutual information, is used as an intensity-based image similarity measure. Registration is performed by searching for the deformation that minimizes a cost function consisting of a weighted combination of the image similarity measure and a regularization term. The novel regularization term is a local volume-preservation (incompressibility) constraint, which is motivated by the assumption that soft tissue is incompressible for small deformations and short time periods. The incompressibility constraint is implemented by penalizing deviations of the Jacobian determinant of the deformation from unity. We apply the nonrigid registration algorithm with and without the incompressibility constraint to precontrast and postcontrast magnetic resonance (MR) breast images from 17 patients. Without using a constraint, the volume of contrast-enhancing lesions decreases by 1%–78% (mean 26%). Image improvement (motion artifact reduction) obtained using the new constraint is compared with that obtained using a smoothness constraint based on the bending energy of the coordinate grid by blinded visual assessment of maximum intensity projections of subtraction images. For both constraints, volume preservation improves, and motion artifact correction worsens, as the weight of the constraint penalty term increases. For a given volume change of the contrast-enhancing lesions (2% of the original volume), the incompressibility constraint reduces motion artifacts better than or equal to the smoothness constraint in 13 out of 17 cases (better in 9, equal in 4, worse in 4). The preliminary results suggest that incorporation of the incompressibility regularization term improves intensity-based free-form nonrigid registration of contrast-enhanced MR breast images by greatly reducing the problem of shrinkage of contrast-enhancing structures while simultaneously allowing motion artifacts to be substantially reduced.**

***Index Terms*—B-splines, contrast-enhanced magnetic resonance (MR) breast images, free-form deformation, mutual information, nonrigid registration, volume preservation.**

Manuscript received July 2, 2002; revised January 7, 2003. The work of T. Rohlfing was supported in part by the National Science Foundation under Grant EIA-0 104 114. A preliminary version of this paper was presented at the Medical Image Computing and Computer-Assisted Intervention Conference (MICCAI), Utrecht, The Netherlands, October 14–17, 2001. *Asterisk indicates corresponding author.*

T. Rohlfing is with the Image Guidance Laboratories, Department of Neurosurgery, Stanford University, Stanford, CA 94305-5327 USA.

*C. R. Maurer, Jr. is with the Image Guidance Laboratories, Department of Neurosurgery, Stanford University, 300 Pasteur Drive, Room S-012, MC 5327, Stanford, CA 94305-5327 USA (e-mail: calvin.maurer@igl.stanford.edu).

D. A. Bluemke and M. A. Jacobs are with the Department of Radiology, The Johns Hopkins University, Baltimore, MD 21218 USA.

Digital Object Identifier 10.1109/TMI.2003.814791

I. Introduction

NONRIGID image registration is becoming a valuable tool for various medical image processing applications [14], [17], [36]. One application of particular clinical interest is the registration of pairs of images acquired before and after contrast administration [11], [19], [23], [25], [32], [37]. A major problem with intensity-based nonrigid registration techniques is that when they are applied to precontrast and postcontrast image pairs, they often produce transformations that substantially change (generally decrease, but sometimes increase) the volume of contrast-enhancing structures. Contrast enhancement is an intensity inconsistency between the two images, which is what intensity-based registration algorithms are designed to minimize. Given that the image intensity might change after injection of the contrast agent, one cannot use a direct comparison of image intensities, i.e., sum of squared intensity differences or correlation, as an image similarity measure. Mutual information, which is based on information theory and was proposed independently in [9] and [50], is an alternative similarity measure that has been shown to accurately and robustly align head images from the same patient that are acquired from different image modalities and differ by a rigid transformation [52]. But although mutual information is an effective similarity measure for rigid registration, it does not prevent contrast-enhancing structures from substantially changing size in nonrigid registration: Tanner *et al.* [44] documented that contrast-enhancing lesions often shrink substantially in contrast-enhanced magnetic resonance (MR) breast images, and we observed the same behavior for contrast-enhancing vessels in three-dimensional (3-D) digital subtraction angiography using X-ray computed tomography head-and-neck images [32]. This problem severely affects the use of the resulting transformation for image subtraction, volumetric analysis, multispectral classification, and pharmacokinetic modeling.

Intensity-based nonrigid image registration is inherently an ill-posed problem. Like many other problems in computer vision and image analysis, registration can be formulated as an optimization problem whose goal is to minimize an associated energy or cost function that consists of a first term that characterizes the similarity between the source and target images and a second term that characterizes the cost associated with particular deformations. The first term is the driving force behind the registration process and aims to maximize the similarity between the two images. The second term,

which is often referred to as the regularization or penalty term, constrains the transformation between the source and target images. Some authors use a smoothness constraint penalty term (sometimes called the biharmonic or thin-plate model term) that is proportional to the deflection bending energy of a thin plate [3], [37], [46], [51]. Others use a penalty term (sometimes called the Laplacian or membrane model term) that is proportional to the deflection energy of a membrane [1], [20], [46]. Christensen *et al.* [7] simultaneously compute, and enforce consistency between, forward and backward transformations between two images. Since this alone does not ensure smoothness, they incorporate an additional linear elastic constraint. Hayton *et al.* [19] use a modified Horn & Schunck [20] optical flow algorithm with a constraint based on a pharmacokinetic model of the contrast uptake. The goodness of fit of the uptake model provides a consistency criterion for the registration. None of these regularization approaches, however, addresses the specific problem of volume loss in the nonrigid registration of contrast-enhanced images.

A different approach specifically designed to address the problem of volume loss couples the control points of a free-form (B-spline) deformation in order to make the contrast-enhancing lesion locally rigid [44]. Little *et al.* [22] incorporate independent rigid structures (in this case vertebral bodies) in a modified thin-plate spline nonrigid registration. These approaches require identification of the rigid structures prior to or during registration. Also, because the structures are considered (and enforced to be) rigid, these approaches prevent deformation of the structures even in cases where they have actually deformed.

More detailed physical models can be used. Edwards *et al.* [12] model two-dimensional (2-D) deformation of the brain during surgery using a three-component model consisting of rigid, elastic, and fluid structures. They propose a number of different energy terms to constrain the deformation, including tension, stiffness, and folding energy terms. Hagemann *et al.* [16] apply a two-tissue model of the human head for nonrigid image registration that aims to model the actual mechanical properties of brain tissue. Although both methods, which were originally described in 2-D, generalize to 3-D, and the latter also to arbitrary numbers of tissues, their computational expense is very high in 3-D. In general, the creation of a discrete mechanical model of an object requires identification of the respective tissue types and assignment of the respective tissue properties before registration. This can be difficult and time consuming and it may not always be possible.

On the other end of the spectrum, purely mathematical strategies can be used to regularize the computed nonrigid transformations. Thirion [49], for example, alternates between optical flow-based computation of motion and Gaussian smoothing of the resulting deformation field. Obviously, this method does not incorporate any prior knowledge about the physical properties of the imaged objects.

In this paper, we choose an approach that does not require any segmentation or tissue identification. We extend the intensity-based nonrigid registration algorithm developed by Rueckert *et al.* [37] by using a novel physics-based regularization term to constrain the deformation. Global motion is modeled by a rigid transformation while local motion is described by a free-form deformation based on B-splines. An information theoretic measure, normalized mutual information, is used as an intensity-based image similarity measure. Registration is performed by searching for the deformation that minimizes a cost function consisting of a weighted combination of the image similarity measure and a regularization term. The novel regularization term is a local volume-preservation (incompressibility) constraint, which is motivated by the assumption that soft tissue is incompressible for small deformations and short time periods. That is, the tissue can be deformed locally, but like a gelatin-filled balloon, the volume (local and total) remains approximately constant. The incompressibility constraint is implemented by penalizing deviations of the Jacobian determinant of the deformation from unity.

The Jacobian determinant has been used previously for analyzing nonrigid transformations [18], [44]. It has been applied to preserve total gray-level intensity (mass) between original and deformed images [5], [13], [24], [41]. The Jacobian determinant can also be used to check for folding. Christensen *et al.* [6], [8] perform automatic regridding in a hierarchical nonrigid registration algorithm by propagating templates as the transformations evaluated on the finite spatial lattice become singular. New templates are generated when the Jacobian of the transformation of the current template drops below 0.5. Christensen and Johnson [7] monitor the Jacobian during their forward-and-reverse consistent image registration to insure that the nonrigid transformation is one-to-one and, therefore, has an inverse (if the Jacobian is positive, the transformation is locally one-to-one), and they suggest that it is also possible to use the Jacobian determinant to penalize substantial compressions and expansions (small and large values of the Jacobian determinant, respectively).[1] Constraint of object deformation based on the Jacobian determinant of free-form deformations has been applied to achieve volume preservation during interactive deformation of volumetric models [31]. The present paper (including an earlier preliminary presentation [32]) is the first work we are aware of that uses the Jacobian determinant in a volume-preservation (incompressibility) regularization term to constrain the coordinate transformation during intensity-based nonrigid image registration.

In physical models that represent the object by a triangular (2-D) or tetrahedral (3-D) mesh, volume preservation can be achieved by adding a constraint term that penalizes deviation in the sizes of the mesh elements (areas of triangles in 2-D [12], volumes of tetrahedra in 3-D [47]). Nonrigid registration can also be performed by modeling the deformation of the source image into the target image as an elastic physical process [2], [10]. The behavior of the elastic body is described by the Navier linear elastic partial differential equation. This equation has two Lamé elasticity constants, which can be interpreted in terms of Young's modulus and Poisson's ratio. A value of 0.5 for Poisson's ratio, which is the ratio between lateral shrinking and

[1]Since these authors are interested in intersubject registration rather than intrasubject registration, they are not interested in an incompressible transformation.

longitudinal stretching, means the material is incompressible. In practice, a value slightly less than 0.5 is used to prevent mesh lock. Although such biomechanical models can be formulated with inherent volume preservation, they require segmentation of tissue types and assignment of tissue properties, neither of which are required in our approach.

To evaluate the efficacy and robustness of our volume-preservation constraint and investigate its potential clinical value, we apply an intensity-based nonrigid registration algorithm with and without the constraint to precontrast and postcontrast MR breast images from 17 patients. The motion artifact reduction and volume-preservation properties of the new constraint are compared with those of a smoothness constraint by blinded assessment of maximum intensity projections of subtraction images.

II. Image Registration Algorithm

Registration is the determination of a geometrical transformation or mapping from points in one image to points in another image. To the extent that corresponding points are mapped together, the registration is successful. In the case of contrast-enhanced MR breast imaging, the goal is to map points in the postcontrast image to the corresponding points in the precontrast reference image. If the transformation is accurate, the registered images can be used for image subtraction, volumetric analysis, multispectral classification, or pharmacokinetic modeling of contrast uptake.

A. Transformation Model

An initial alignment of precontrast and postcontrast images is achieved using an intensity-based rigid registration algorithm with six parameters (three for rotation, three for translation). Our method is an independent implementation [35] of the rigid registration algorithm described in [42]. It uses normalized mutual information (NMI) as the image similarity measure [43]. In the first step, this method is used to find a rigid transformation to describe the global motion of the object. The rigid transformation is then used as the initial estimate for the nonrigid registration.

The intensity-based nonrigid registration algorithm is an independent and modified implementation of the technique introduced by Rueckert *et al.* [37]. The algorithm determines the set of parameters of a deformation $\mathbf{T}$ that optimizes the cost function in (4), which is described in Section II-B.

The transformation model is a multilevel formulation [21] of a free-form deformation based on cubic B-splines [40]. The basic idea of a free-form deformation is to deform an object by manipulating an underlying mesh of control points. The transformation $\mathbf{T}$ is defined by a control point grid (CPG) Φ, a lattice of uniformly spaced control points $\phi_{i,j,k}$, where $-1 \leq i < n_x-1, -1 \leq j < n_y-1$, and $-1 \leq k < n_z-1$. Control points with i, j, or k equal to either 0 or n_x-3 (n_y-3 and n_z-3 for j and k, respectively) are located on the edge of the image data. The spacings between the control points in x, y, and z directions are denoted by δ_x, δ_y, and δ_z, respectively. By moving the control points independently of each other, the space between them is deformed nonrigidly. At any position $\mathbf{x} = (x, y, z)$ the deformation is computed from the positions of the surrounding $4 \times 4 \times 4$ neighborhood of control points

$$\mathbf{T}(\mathbf{x}) = \sum_{l=0}^{3} \sum_{m=0}^{3} \sum_{n=0}^{3} B_l(u) B_m(v) B_n(w) \phi_{i+l,j+m,k+n}. \quad (1)$$

Here, i, j, and k denote the index of the control point cell containing $\mathbf{x} = (x, y, z)$, and u, v, and w are the relative positions of x, y, and z, respectively, inside that cell in the three dimensions, e.g., $i = \lfloor x/\delta_x \rfloor - 1$ and $u = x/\delta_x - (i+1)$. The functions B_0 through B_3 are the approximating third-order spline polynomials as described in [21]

$$\begin{aligned} B_0(t) &= (-t^3 + 3t^2 - 3t + 1)/6 \\ B_1(t) &= (3t^3 - 6t^2 + 4)/6 \\ B_2(t) &= (-3t^3 + 3t^2 + 3t + 1)/6 \\ B_3(t) &= t^3/6. \end{aligned} \quad (2)$$

The parameters of a B-spline based transformation are the coordinates of the control points $\phi_{i,j,k}$. In comparison to Rueckert *et al.* [37], our approach does not consider these vectors to be offsets from the original control point positions with initial displacements of zero. Instead, we use them as absolute positions and initialize them as $\phi^{(0)}_{i,j,k} := (i\delta_x, j\delta_y, k\delta_z)$. Thus, the coordinate transformation is $\mathbf{x} \mapsto \mathbf{T}(\mathbf{x})$ rather than $\mathbf{x} \mapsto \mathbf{x} + \mathbf{T}(\mathbf{x})$. This makes application of the actual deformation computationally more efficient for two reasons: First of all, it immediately reduces the number of required real-value additions per transformed coordinate by three. More importantly, $\mathbf{T}$ is linear with respect to the $\phi_{i,j,k}$. Therefore, an initial rigid transformation A can be incorporated by applying it to the control point positions ϕ and working with transformed control points ϕ^A instead

$$\begin{aligned} &(A \circ \mathbf{T})(\mathbf{x}) \\ &\quad = \sum_{l,m,n=0}^{3} B_l(u) B_m(v) B_n(w) (A\phi_{i+l,j+m,k+n}) \\ &\quad = \sum_{l,m,n=0}^{3} B_l(u) B_m(v) B_n(w) \phi^A_{i+l,j+m,k+n}. \end{aligned} \quad (3)$$

As a consequence, the computational cost for every transformed vector is reduced by the cost of a vector-matrix multiplication plus another vector addition. By implicitly applying the rigid transformation *after* the deformation, we ensure that this is mathematically equivalent to explicitly applying A (because computation of i, j, k, u, v, and w remains independent of A).

The basis functions of the cubic B-splines that define the geometrical transformation model described above have two mathematical properties relevant for the present paper: they have a limited support (i.e., changing the position of a control point affects the transformation only in the $4 \times 4 \times 4$ neighborhood of the control point), and they are $\mathcal{C}^2$ continuous. The first property allows for efficient computation of the transformation [33], while the second property allows for the analytical computation of continuous first- and second-order derivatives. The latter property ensures that the deformation constraints described below, since they are based on first- and second-order derivatives, can be efficiently computed and are,

in fact, continuous functions themselves, which is important for effective optimization.

B. Cost Function

In addition to the NMI similarity measure E_{NMI}, our registration method incorporates an additional penalty term $E_{\mathrm{constraint}}$ to constrain the deformation of the coordinate space. A user-defined weighting factor $\omega\,(0 \leq \omega < 1)$ controls the relative influence of E_{NMI} and $E_{\mathrm{constraint}}$, combining both into the overall cost function E_{total} as follows:

$$E_{\mathrm{total}} = (1-\omega)E_{\mathrm{NMI}} - \omega E_{\mathrm{constraint}}. \tag{4}$$

In this formula, the constraint term has a negative sign, because the aim of the registration is to *maximize* image similarity, whereas it is supposed to *minimize* the volume change quantified by the constraint. The general idea of constrained optimization is to regularize (or stabilize) an otherwise ill-posed problem by combining a data-dependent term (E_{NMI}) with a term that incorporates *a priori* knowledge about the underlying problem. While the data-dependent term favors solutions that agree with the actual observations, the constraint term favors nondegenerate solutions. The constraint is, therefore, also often referred to as a *regularizer* or *stabilizer*. We note that in our approach, unlike the numerical literature [29], [48], both components of the overall cost function are weighted in a way that allows us to exclusively optimize either of its two parts without requiring nonfinite values for the weight ω.

This paper considers two different constraint terms as possible choices for $E_{\mathrm{constraint}}$, each modeling a different physics-based property of the deformation. Both constraints can easily be computed directly from the nonrigid coordinate transformation. In Section II-C, we introduce a novel volume-preserving (incompressibility) deformation constraint, denoted E_{Jacobian}, which is based on the assumption that tissue is incompressible. This constraint is implemented using the Jacobian determinant of the deformation. In Section II-D, we review a smoothness constraint E_{smooth}, which is based on the bending energy of a thin plate subjected to bending deformations but has no inherent volume-preservation properties.

C. Incompressibility Constraint

The design of our deformation constraint is motivated by the observation that many tissues in the human body, including the breast, are approximately incompressible for small deformations and short time periods. In a small neighborhood of the point $\mathbf{x}$, the local compression or expansion caused by the deformation $\mathbf{T}$ can be calculated by means of the Jacobian determinant

$$J_{\mathbf{T}}(\mathbf{x}) = \det \begin{pmatrix} \frac{\partial \mathbf{T}_x(\mathbf{x})}{\partial x} & \frac{\partial \mathbf{T}_x(\mathbf{x})}{\partial y} & \frac{\partial \mathbf{T}_x(\mathbf{x})}{\partial z} \\ \frac{\partial \mathbf{T}_y(\mathbf{x})}{\partial x} & \frac{\partial \mathbf{T}_y(\mathbf{x})}{\partial y} & \frac{\partial \mathbf{T}_y(\mathbf{x})}{\partial z} \\ \frac{\partial \mathbf{T}_z(\mathbf{x})}{\partial x} & \frac{\partial \mathbf{T}_z(\mathbf{x})}{\partial y} & \frac{\partial \mathbf{T}_z(\mathbf{x})}{\partial z} \end{pmatrix}. \tag{5}$$

The value of $J_{\mathbf{T}}(\mathbf{x})$ is equal to one if the deformation at $\mathbf{x}$ is incompressible, greater than one if there is local expansion, and less than one if there is compression. Since the 3-D spline is the tensor product of independent one-dimensional (1-D) functions, its derivative with respect to x is computed as follows:

$$\frac{\partial \mathbf{T}_x(\mathbf{x})}{\partial x} = \frac{1}{\delta_x} \sum_{l,m,n=0}^{3} \frac{dB_l(u)}{du} B_m(v) \times B_n(w)\phi_{i+l,j+m,k+n}. \tag{6}$$

The remaining derivatives have an analogous form. Computation of the entries of $J_{\mathbf{T}}(\mathbf{x})$ is in fact very similar to computing $\mathbf{T}$ itself. Depending on the position in the matrix, the spline polynomials $B_{0,1,2,3}$ in the respective dimension are replaced by their respective derivatives. These derivatives are easily computed analytically

$$\begin{aligned} dB_0(t)/dt &= (-t^2+2t-1)/2 \\ dB_1(t)/dt &= (3t^2-4t)/2 \\ dB_2(t)/dt &= (-3t^2+2t+1)/2 \\ dB_3(t)/dt &= t^2/2. \end{aligned} \tag{7}$$

The incompressibility constraint penalty term is defined as the integral of the absolute logarithm of the Jacobian determinant, integrated over the domain V_R of the reference image

$$E_{\mathrm{Jacobian}} = \int_{V_R} |\log(J_{\mathbf{T}}(\mathbf{x}))|\, d\mathbf{x}. \tag{8}$$

This term penalizes local deviations of $J_{\mathbf{T}}(\mathbf{x})$ from unity, that is, it penalizes local tissue expansion and compression.[2] The penalty term is nonnegative and has its minimum value of zero when the value of $J_{\mathbf{T}}(\mathbf{x})$ is unity, i.e., when the deformation at $\mathbf{x}$ is incompressible. Alternative forms of the constraint term are possible, e.g., $\int_{V_R} |J_{\mathbf{T}}(\mathbf{x})-1| d\mathbf{x}$. One motivation for using the absolute logarithm of the Jacobian determinant is to symmetrically weight local expansion and compression [4], and to assign zero penalty for local volume preservation. A different form that also satisfies these criteria is $\int_{V_R} (J_{\mathbf{T}}(\mathbf{x}) + 1/J_{\mathbf{T}}(\mathbf{x}) - 2)\, d\mathbf{x}$. Yet another alternative form of the constraint term is $\left| \int_{V_R} (J_{\mathbf{T}}(\mathbf{x}) - 1)\, d\mathbf{x} \right|$, which penalizes only global volume change rather than the local effects detected by (8). However, this alternative global volume-preserving constraint would allow the deformation to shrink a contrast-enhancing structure and compensate for this by simultaneously expanding a background region, which is obviously not the kind of behavior we are after.

As a discrete approximation to the continuous integral in (8), the average of the proposed incompressibility constraint is computed over a finite set D of samples which uniformly cover the reference image:

$$E_{\mathrm{Jacobian}} = \frac{1}{N_D} \sum_{\mathbf{x} \in D} |\log(J_{\mathbf{T}}(\mathbf{x}))|. \tag{9}$$

One possible choice for D is the set of all control points of the deformation for which the original positions $\phi^{(0)}_{i,j,k}$ are inside or on the edge of the reference image. For these points, evaluation of the Jacobian determinant is particularly efficient as the values

[2]The constraint term can be easily generalized to the situation in which a global scaling between the image is required (e.g., because one of the images needs to be corrected for scaling errors in the imaging process) by dividing the Jacobian determinant in (8) by a global scaling factor.

of the B-spline functions and their derivatives are the same at all control points and, hence, can be precomputed. But the CPG is typically much less densely sampled than, for example, the voxel grid of the images and, thus, the Jacobian is evaluated at a rather small number of locations. The coordinates of the $X \times Y \times Z$ voxels of the reference image are, therefore, another natural choice for D that has in our work provided better numerical stability of the constraint computation

$$D_R = \{\mathbf{x}_{i,j,k} : 0 \leq i < X, 0 \leq j < Y, 0 \leq k < Z\}. \quad (10)$$

Some important properties of the penalty term E_{Jacobian} should be noted. First, as calculation of the entries in the Jacobian matrix is very similar to computing $\mathbf{T}$ itself, many terms can be precomputed [33]. Therefore, E_{Jacobian} can be computed very efficiently, which is important to keep execution time reasonable. Second, since every control point affects $\mathbf{T}$ only within its immediate neighborhood, the discrete approximation to the derivatives of E_{Jacobian} with respect to the control point coordinates can also be computed very efficiently. For finite-difference approximation to this derivative, a small offset ϵ is added to and subtracted from the respective parameter. The penalty term E_{Jacobian} is then reevaluated, yielding E^{+}_{Jacobian} and E^{-}_{Jacobian}. As all terms in (9) outside a $4 \times 4 \times 4$ neighborhood of the affected control point are constant, they cancel out when $\Delta E_{\text{Jacobian}} = (E^{+}_{\text{Jacobian}} - E^{-}_{\text{Jacobian}})/2\epsilon$ is calculated. Computation can, thus, be restricted to the interior of this region.

D. Smoothness Constraint

A different regularization approach is to constrain the deformation to be smooth by adding a biharmonic model penalty term, which is based on the bending energy of a thin plate of metal that is subjected to bending deformations [3], [37], [46], [51]. The penalty term is composed of second-order derivatives of the deformation

$$E_{\text{smooth}} = \int_D \left(\frac{\partial^2 \mathbf{T}}{\partial x^2}\right)^2 + \left(\frac{\partial^2 \mathbf{T}}{\partial y^2}\right)^2 + \left(\frac{\partial^2 \mathbf{T}}{\partial z^2}\right)^2 + 2\left[\left(\frac{\partial^2 \mathbf{T}}{\partial x \partial y}\right)^2 + \left(\frac{\partial^2 \mathbf{T}}{\partial y \partial z}\right)^2 + \left(\frac{\partial^2 \mathbf{T}}{\partial z \partial x}\right)^2\right] d\mathbf{x}. \quad (11)$$

Just like the first-order derivatives of the B-spline transformation, the second-order derivatives are computed by substituting the appropriate derivatives for the corresponding polynomials. Differentiating twice with respect to the same variable results in substituting one spline polynomial by its second-order derivative, e.g.,

$$\frac{\partial^2 \mathbf{T}(\mathbf{x})}{\partial x^2} = \frac{1}{\delta_x^2} \sum_{l,m,n=0}^{3} \frac{d^2 B_l(u)}{du^2} B_m(v) \times B_n(w) \phi_{i+l,j+m,k+n}. \quad (12)$$

The second-order spline derivatives are easily computed analytically from the first-order derivatives in (7). Mixed second-order derivatives with respect to two different variables are computed by substituting two spline polynomials with their respective first-order derivatives, e.g.,

$$\frac{\partial^2 \mathbf{T}(\mathbf{x})}{\partial x \partial y} = \frac{1}{\delta_x \delta_y} \sum_{l,m,n=0}^{3} \frac{dB_l(u)}{du} \frac{dB_m(v)}{dv} \times B_n(w) \phi_{i+l,j+m,k+n}. \quad (13)$$

Just as with the incompressibility constraint introduced in the previous section, the continuous integral in (11) is approximated as a discretely sampled sum over a set of points D

$$E_{\text{smooth}} = \frac{1}{N_D} \sum_{\mathbf{x} \in D} Q_{\mathbf{T}}(\mathbf{x}). \quad (14)$$

In the interest of notational simplicity, $Q_{\mathbf{T}}(\mathbf{x})$ denotes the sum of squared second-order derivatives of $\mathbf{T}$ inside the integral in (11), evaluated at the location $\mathbf{x}$. Regarding the computation of the derivatives with respect to the parameters of the free-form deformation, the same observations that applied to E_{Jacobian} are also true for E_{smooth}. This means that the derivative approximation with finite differences can be restricted to the local neighborhood of the control point affected by the current parameter.

E. Optimization

Finding the parameters of the nonrigid transformation that optimize the joint cost function E_{total} requires an efficient and robust optimization algorithm. We are using a method similar to the optimization strategy described by Rueckert *et al.* [37]: the gradient of the cost function is computed, and a simple line search (downhill–simplex algorithm [26] restricted to the direction of the steepest ascent; see [35] for a full description of our method) is performed for the optimum parameters along the gradient direction. Note that the gradient can be estimated very efficiently due to the local effect of the control point positions. This procedure is repeated until the cost function cannot be improved any further. Like Rueckert *et al.*, we aim to improve robustness and efficiency of the registration algorithm by employing a multiresolution approach, starting with a coarse CPG spacing that is successively refined using a B-spline subdivision algorithm [15], [21], [32], [35], [37].

We reduce the number of degrees of freedom of the nonrigid transformation by excluding deformation control points in the image background from all computations [32], [35], which is similar to a strategy described independently by Schnabel *et al.* [38]. This can safely be done because each control point influences only its local $4 \times 4 \times 4$ neighborhood. Therefore, if this neighborhood covers nothing but image background, then the respective control point has no influence on the registration of the imaged objects. We identify background regions using a simple entropy-based criterion [32], [35]. In short, a control point is excluded from computation if, in both the reference and the target image, the local entropy of its $4 \times 4 \times 4$ neighborhood is less than 50% of the entropy of the respective image as a whole. In practice, we have found this simple criterion to work very well. Importantly, we have never experienced it to exclude control points in the image foreground.

Some additional implementation details help to further increase computational efficiency: when one control point is moved for computation of the gradient of E_{NMI}, a local 2-D histogram is computed from that point's local neighborhood and compounded with a precomputed global histogram [41]. Also, since the nonrigid transformation is a tensor product of 1-D B-spline functions, we can evaluate it by voxel rows in the reference image (i.e., parallel to the x axis of the coordinate system) and precompute the tensor components in the y and z directions (see [33] for the mathematical details). Finally, a parallel (multithreaded) implementation [33] allows us to take advantage of modern multiprocessor workstations and shared-memory supercomputers.

III. Study Design

A. Image Data

Seventeen patients (age range, 18–80 years; median, 45 years) were consecutively referred for MR evaluation of suspicious findings and/or extent of the breast lesion. After MR image acquisition and evaluation, either core or excisional biopsies were performed on some patients ($n = 14$); the remaining patients underwent surgical incision/lumpectomy or mastectomy ($n = 3$). A lesion was diagnosed by analysis of histological sections. The lesions were diagnosed as malignant for 11 patients and benign for the other 6.

We applied the nonrigid registration algorithm presented in this paper to MR breast images acquired before and after contrast injection. The MR scans were performed on a 1.5 T MR scanner (General Electric Medical Systems, Milwaukee, WI), using a dedicated phased array breast coil (MRI Devices, Waukesha, WI) with the patient lying prone with the breast in a holder to reduce motion. Fat-suppressed 3-D T_1-weighted FSPGR ($T_R = 20$ ms, $T_E = 4$ ms, $\mathrm{FOV} = 18 \times 18$ cm, $\mathrm{matrix} = 512 \times 160, 60$ slices, $\mathrm{slice\ thickness} = 2$ mm) precontrast and postcontrast images were obtained after intravenous administration of gadopentetate dimeglumine (Gd-DTPA) contrast agent (Magnevist, Berlex, Wayne, NJ; patients received 0.1 mmol/kg as 0.2 ml/kg of 0.5 mol/l contrast solution). The contrast agent was hand injected over 10 s with MR imaging beginning immediately after completion of the injection. The contrast bolus was then followed by a 20-cc flush. The breast lesion was defined by contrast enhancement and identified by a radiologist.

B. Registration

Each pair of precontrast and postcontrast images was first registered using a rigid transformation. Given the rigid registration as the initial alignment, various nonrigid registrations were then computed. An unconstrained free-form deformation provided reference for artifact reduction and volume loss. Constrained free-form deformations were computed, covering a large range of weighting factors for the deformation constraint ($10^{-4} \leq \omega < 1$). The incompressibility constraint introduced in Section II-C and the smoothness constraint reviewed in Section II-D were used independently in order to compare their effectiveness. The constraint terms were evaluated at all voxel locations in order to achieve maximum numerical stability [Section II-C, in particular (10)]. All nonrigid registrations started with a 40 mm control point spacing that was hierarchically (successively) refined using a B-spline subdivision algorithm [15], [21], [32], [35], [37] to 20 mm, 10 mm, and finally 5 mm. In parallel, the image data resolution was refined from a 4 mm voxel size to 2 mm, 1 mm, and at the final stage the original image data was used.

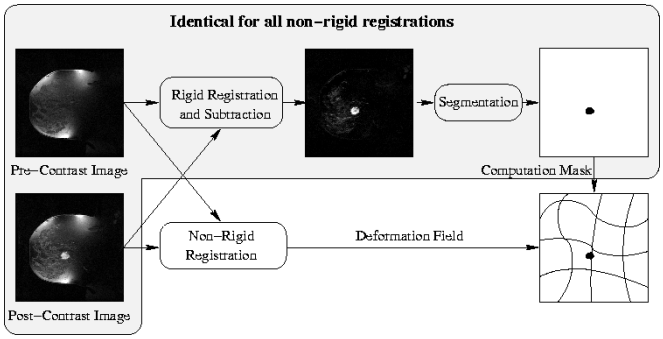

Fig. 1. Measurement of the relative volume change of contrast-enhancing structures after nonrigid registration. A mask to compute the local volume change of contrast-enhancing structures is generated by segmenting the subtraction image after rigid registration. The mask is expressed in the coordinates of the precontrast image and is the same for all nonrigid transformations to be evaluated.

C. Measurement of Volume Change

One possible way of quantifying the change of volume of contrast-enhancing structures before and after nonrigid registration is to segment them in the resulting subtraction images and compare the resulting volumes. However, this introduces inaccurate segmentation as an additional source of error. Instead, we segment only once and apply the nonrigid coordinate transformation itself to quantify the local volume change. The process of measuring the volume change of contrast-enhancing structures is illustrated in Fig. 1.

The structures of interest are identified in the subtraction image after rigid registration by a region growing method, resulting in a set C_0 of contrast-enhancing voxels. We then use the nonrigid coordinate transformation $\mathbf{T}$ to compute the set of contrast-enhancing voxels $C_{\mathbf{T}}$ after deformation. The relative volume c_v of the segmented contrast-enhancing region after deformation is then easily computed as the ratio of the voxel counts $c_v = |C_{\mathbf{T}}|/|C_0|$. If $c_v < 1$, the fractional contrast-enhancing volume decrease is $1 - c_v$, else the fractional volume increase is $c_v - 1$. As the precontrast image is the reference image for all registrations, the contrast-enhancing region segmented in the subtraction image after rigid registration is defined in the coordinate system of the precontrast image. The *inverse* of the rigid transformation between precontrast and postcontrast image, therefore, needs to be concatenated with the nonrigid transformation, which maps *from* the precontrast *to* the postcontrast image, in order to compute the correct deformed region.

Segmentation of the contrast-enhancing structures in the subtraction image is subject to segmentation error. Also, the particular volume of interest in the precontrast and postcontrast image

is not generally in perfect alignment after rigid registration, resulting in an additional potential error when identifying the contrast-enhancing structures of interest. However, these structures are segmented only once. Furthermore, C_0 is defined in the coordinate system of the precontrast image that serves as the common reference image of all rigid and nonrigid registrations. The volume C_0 is, therefore, identical for all transformations analyzed for one particular patient (Fig. 1). The analysis is, thus, not affected by different segmentations in the different subtraction images. It may be biased, but the bias is constant for all transformations analyzed.

It should be emphasized that the sole purpose of segmenting the contrast-enhancing structures in the context of the present paper is the retrospective analysis of volume changes. It is neither necessary for nor part of the registration process itself.

D. Assessment of Registration Quality

It is not a trivial task to give a quantitative assessment of the registration quality, e.g., the capability of the constrained registration algorithm to eliminate motion artifacts. Values for the image similarity measure component of the combined cost function can easily be computed, but carry no objective meaning. Also, it is obvious that the image similarity can be improved by allowing contrast-enhancing structures to disappear. This, however, is clearly not desirable. We, therefore, resist providing numerical values of image similarities and rely on visual inspection of the subtraction images instead.

One question to answer is whether the proposed technique provides a general way of compensating motion artifacts in subtraction imaging while preventing volume loss of contrast-enhancing structures. For both constraints and for each individual patient, we independently determined the smallest weighting factor for the respective constraint term that provided volume preservation of the identified lesion within 2% of the original volume. Using the nonrigid transformation computed with this weighting factor, a 3-D subtraction image was generated and rendered by maximum intensity projection (MIP). Likewise, MIP images were generated from subtraction images resulting from rigid and from unconstrained nonrigid registration.

The four resulting MIP images per patient were randomized and presented to an experienced observer. The blinded observer ranked the subtraction MIP images based on motion artifact reduction, assigning rank #1 to the subtraction image showing the fewest artifacts and assigning rank #4 to the image showing the most residual artifacts. Several images could be assigned the same rank, in which case an appropriate number of subsequent ranks was left unassigned (e.g., if one image clearly has the fewest artifacts, another has the most artifacts, and the remaining two images are indistinguishable, the rankings are #1, #2, #2, and #4).

IV. Results

A. General Observations

The original volumes of the contrast-enhancing structures in the images from 17 patients ranged from 0.2 to 77.7 ml ($\text{mean} \pm \text{SD} = 9.1 \pm 19.0$ ml). These volumes were determined by semi-automatically segmenting the contrast-enhancing structures in the subtraction image after rigid registration.

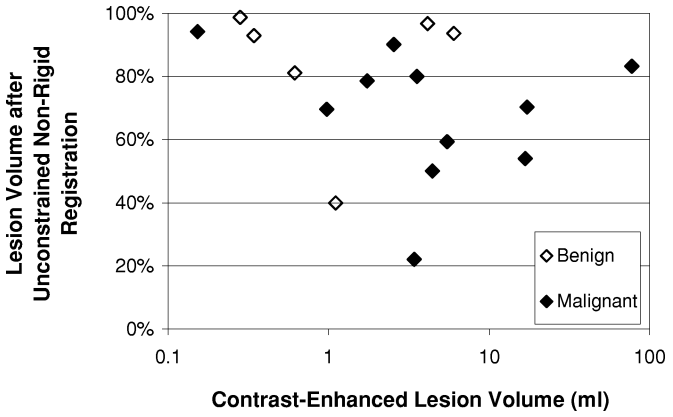

Fig. 2. Scatter plot of relative lesion volume after registration vs. original lesion volume. The volume of the contrast-enhancing structure is on the horizontal log-scale axis. The relative volume (in percent) after registration is shown on the linear vertical axis. The correlation between relative lesion volume and original lesion volume is not significant ($R^2 < 0.001, P = 0.91$).

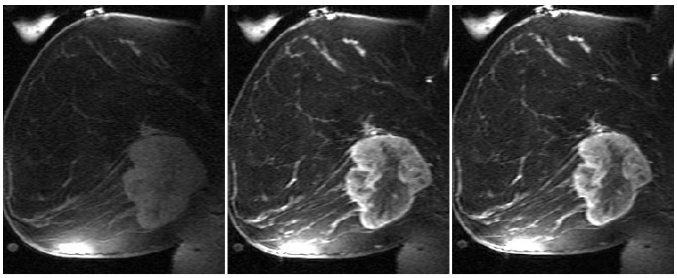

Fig. 3. Example of a contrast-enhancing structure that is also visible in the precontrast image. (a) Precontrast image. (b) Corresponding postcontrast slice after rigid registration. (c) Corresponding postcontrast slice after unconstrained nonrigid registration. This very large lesion (77.7 ml) shrank by only 17% during unconstrained nonrigid registration.

As other groups have reported before [44], unconstrained intensity-based nonrigid registration of precontrast and postcontrast images often results in substantial volume loss of the contrast-enhancing structures. For the 17 patients analyzed in the present study, volume loss was between 1.3% and 78.0% $(26.1 \pm 22.2\%)$. While it is also possible for contrast-enhancing structures to *expand* during nonrigid registration [44], we did not find any volume increases after unconstrained registrations. We did, however, sometimes observe small volume increases using both deformation constraints (see Section IV-B).

Fig. 2 shows a plot of relative lesion volume after unconstrained nonrigid registration versus original lesion volume. Very small structures (less than 0.5 ml) in two patients had much less volume loss than the vast majority of larger lesions in the other patients. However, there is no relationship between relative volume loss and total lesion volume (linear regression, $R^2 = 0.0012, P = 0.89$, correlation not significant). Instead, our results, based on the 17 available image pairs, suggest the following rules of thumb: A contrast-enhancing structure shrinks less if it is also visible in the precontrast image (Fig. 3) or has an irregular surface (Fig. 4). Lesions that show the

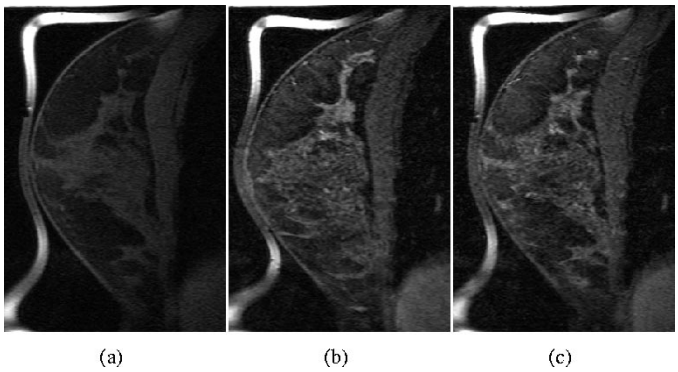

Fig. 4. Example of a contrast-enhancing structure with an irregular shape. (a) Precontrast image. (b) Corresponding postcontrast slice after rigid registration. (c) Corresponding postcontrast slice after unconstrained nonrigid registration. This large lesion (6.1 ml), which also stands out from the surrounding tissue in the precontrast image, shrank by less than 2% during unconstrained nonrigid registration.

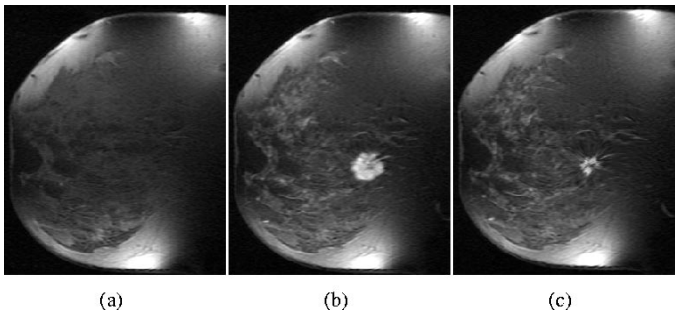

Fig. 5. Example of a small but nearly spherical contrast-enhancing structure. (a) Precontrast image. (b) Corresponding postcontrast slice after rigid registration. (c) Corresponding postcontrast slice after unconstrained nonrigid registration. This lesion, which is relatively small (3.4 ml) and which has little or no contrast relative to the surrounding tissue in the precontrast image, showed the highest relative volume loss, 78%, of all patients in the present study.

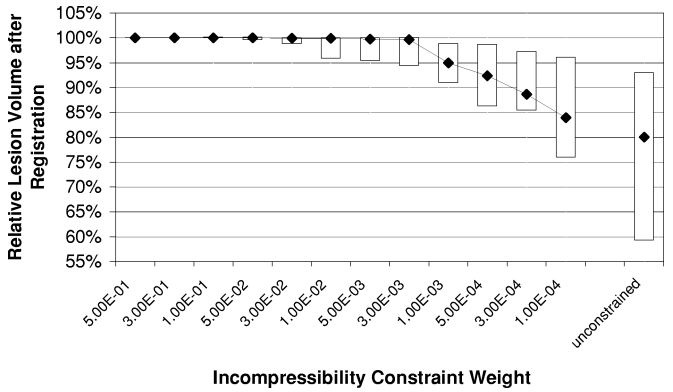

Fig. 6. Distribution of relative volumes of contrast-enhancing structures after nonrigid registration with different weights of the incompressibility constraint E_{Jacobian}. The diamonds show the median values over all 17 patients; upper and lower edges of the boxes show the 25th and 75th percentiles, respectively. The rightmost column shows the values for unconstrained registration as a reference.

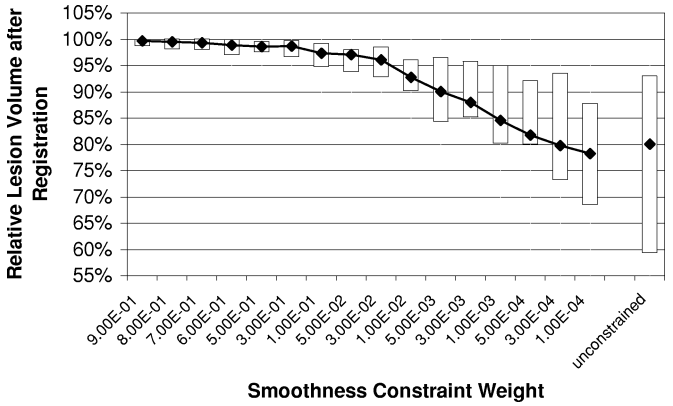

Fig. 7. Distribution of relative volumes of contrast-enhancing structures after nonrigid registration with different weights of the smoothness constraint E_{smooth}. The diamonds show the median values over all 17 patients; upper and lower edges of the boxes show the 25th and 75th percentiles, respectively. The rightmost column shows the values for unconstrained registration as a reference.

highest relative volume loss are typically nearly spherical and have little or no contrast relative to the surrounding tissue in the precontrast image (Fig. 5).

Shape analysis of tumors has previously indicated that typically benign lesions have smooth boundaries, whereas malignant lesion boundaries can be irregular or spiculated [27], [28], [30]. Given our observations outlined above, one might, therefore, suspect that benign lesions, on average, would show higher volume loss than malignant ones. However, at least with the 17 patients in our study, we could not find such a correspondence. For example, a biopsy performed on the patient in Fig. 4 found a benign ductal hyperplasia with microcalcifications; the contrast-enhancing lesion has an irregular shape and shrank less than 2% during unconstrained registration. The patient in Fig. 5 was diagnosed with a malignant infiltrating ductal carcinoma; the lesion has a smooth boundary and shrank 78%. In our limited set of 17 patients, there were no significant correlations between lesion type (benign or malignant) and lesion shape (smooth or irregular), lesion size, or relative lesion volume after unconstrained nonrigid registration.

B. Volume Preservation

On average, for both deformation constraints E_{Jacobian} and E_{smooth}, volume preservation improves as the relative weight of the constraint penalty term increases (Figs. 6 and 7). Although we did not segment and quantitatively analyze contrast-enhancing structures other than the identified tumors (e.g., vessels), we visually observed that the volume of these regions was also relatively well preserved. In MIP renderings of subtraction images, vascular structures appear substantially brighter and more contiguous when the nonrigid transformation is constrained (Fig. 8).

Obviously, the specific weights of both constraints that lead to similar relative volumes cannot be compared with each other. Nonetheless, one can consider how specific the volume-preserving effect is for both constraints. With sufficiently high relative weighting factors, the median volume change of contrast-enhancing structures is less than 1% for both constraints. For the incompressibility constraint, the volume change is less than 1% for all 17 patients over a wide range of weighting factors. This is important because a wide range of weighting factors producing

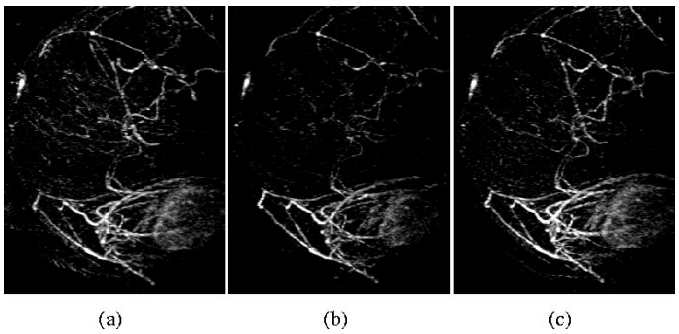

Fig. 8. Volume preservation of vascular structures in MIP renderings of subtraction images. (a) After rigid registration. (b) After unconstrained nonrigid registration. (c) After nonrigid registration with incompressibility constraint. In this example, the use of the incompressibility constraint preserves not only the volume of the contrast-enhancing tumor in the lower right corner of the images (46% volume loss after unconstrained registration). The vascular tree, especially in the center of the images, is also relatively well preserved and visually appears much clearer after the constrained than after the unconstrained registration.

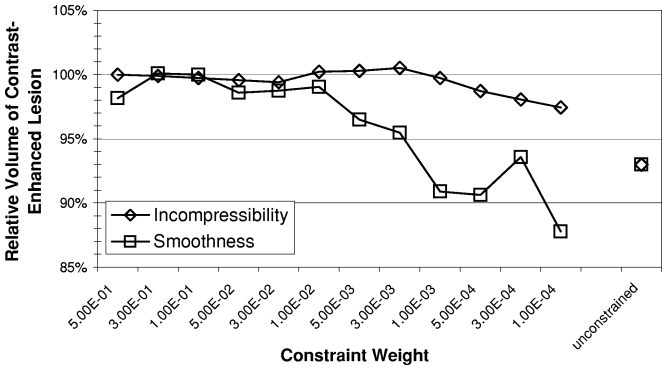

Fig. 9. Relative volume of contrast-enhancing structures in one patient with incompressibility vs. smoothness constraint. The rightmost column is the relative volume after unconstrained registration.

similar volume preservation effects indicates robustness of the constraint with respect to the (heuristic) choice of that factor. However, for the smoothness constraint, no choice of weighting factor kept the volume change less than 1% for all 17 patients.

For individual patients, the improvement of volume preservation with the increase in relative weight of the constraint penalty term is approximately monotonic for the incompressibility constraint, but is often not monotonic for the smoothness constraint. This is illustrated for one patient in Fig. 9. Also, for small weighting factors, registration using the smoothness constraint sometimes caused the contrast-enhancing lesion to shrink even more than registration without any constraint. This behavior was observed in 7 of the 17 patients, including the one patient shown in Fig. 9.

While we did not find any increase in the volume of the contrast-enhancing structures during unconstrained nonrigid registration, the contrast-enhancing lesions in some patients expanded during constrained registration for some values of the constraint weight, in almost all cases by less than 1%. In one patient, however, there was a volume increase of up to 6% for the incompressibility constraint and up to 5% for the smoothness constraint.

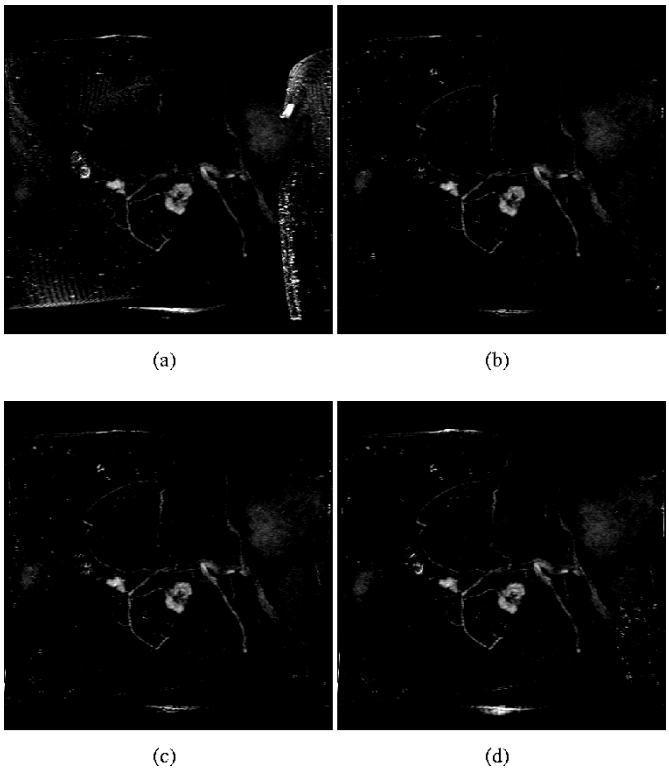

Fig. 10. Maximum intensity projections of subtraction images from one patient. (a) After rigid registration. (b) After unconstrained nonrigid registration (10% volume loss). (c) After nonrigid registration with incompressibility constraint (1% volume loss). (d) After nonrigid registration with smoothness constraint (1% volume loss). All three nonrigid registrations (unconstrained, incompressibility constraint, and smoothness constraint) substantially reduced the motion artifacts that are visible in the rigid registration. In the blinded assessment of motion artifact for this patient, rigid registration was ranked worst (most motion artifact), unconstrained nonrigid registration was ranked best (least motion artifact), and registration with the incompressibility constraint was ranked better than that with the smoothness constraint.

C. Artifact Reduction

On average, for both deformation constraints E_{Jacobian} and E_{smooth}, volume preservation improves, and motion artifact reduction worsens, as the relative weight of the constraint penalty term increases. Thus, there is a tradeoff between volume preservation and motion artifact reduction. Nonetheless, as Fig. 10 illustrates, constrained nonrigid registration can achieve levels of artifact reduction comparable to that produced by unconstrained nonrigid registration. The smoothness constraint typically performs slightly worse than the incompressibility constraint in that, for a given volume loss, the subtraction image obtained using the smoothness constraint generally has more residual artifacts than the image obtained using the incompressibility constraint. This observation is confirmed by the results of the blinded ranking of motion artifact reduction achieved by each constraint (Fig. 11). For both constraints and for each individual patient, we independently determined the smallest weighting factor for the respective constraint penalty term that provided volume preservation of the identified lesion within 2%. Unconstrained nonrigid registration was ranked best (least residual motion artifact) for all 17 patients. Rigid registration was ranked worst (most residual motion artifact) for 16 out of 17 patients. In 9 out of 17 patients, nonrigid registration using the incompressibility constraint was found to achieve better artifact reduction

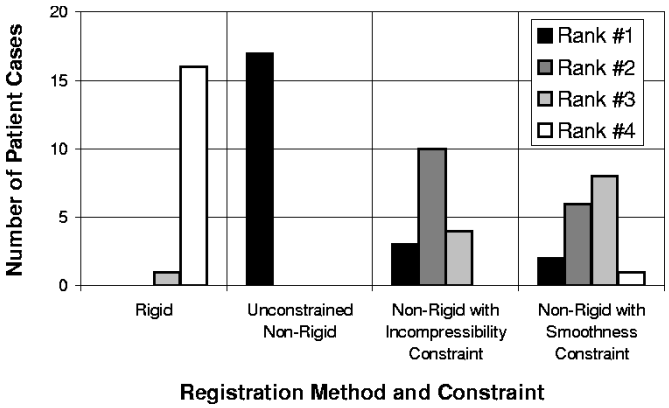

Fig. 11. Histogram plot of artifact reduction rankings. Rank #1 was assigned to the image with least motion artifact.

than the smoothness constraint; in four patients, both constraints were judged equally good; in four patients, the smoothness constraint was judged to achieve better artifact reduction than that of the incompressibility constraint.

V. Discussion

We have presented a novel incompressibility (local volume preservation) constraint for nonrigid registration algorithms. The constraint penalty term, which is based on the Jacobian determinant of the deformation, as well as its discrete derivatives are easy to implement and can be computed efficiently. As a volume-preserving deformation constraint, it is effective and efficient. Its considerable insensitivity to the choice of the weighting factor with respect to the intensity-based similarity measure is an important feature since the two terms in the cost function (the image similarity measure and the constraint penalty term) are fundamentally different entities and, thus, there is no *a priori* correct weighting.

The results from 17 contrast-enhanced MR breast image data sets suggest that incorporation of the incompressibility constraint improves intensity-based nonrigid registration of precontrast and postcontrast images by reducing the problem of shrinkage of contrast-enhancing structures while simultaneously allowing motion artifacts to be substantially reduced. A smoothness constraint was also found to effectively enforce volume preservation in most cases. However, a blinded comparison study showed that the incompressibility constraint performed slightly better than the smoothness constraint. For a given level of volume preservation, the motion artifact reduction achieved using the incompressibility constraint was ranked consistently better than the smoothness constraint.

There is a tradeoff between volume preservation, with constrained registration performing better (as judged by quantitative measurement of volume), and artifact reduction, with unconstrained registration performing better (as judged by visual assessment of artifacts). In the blinded assessment of artifact reduction, we chose to assign a relative rating (i.e., rank) rather than an absolute rating because of the difficulty in assigning an absolute rating. The unconstrained registration consistently produced the fewest artifacts. Nonetheless, the incompressibility constraint, with the weight set such that it preserved the volume

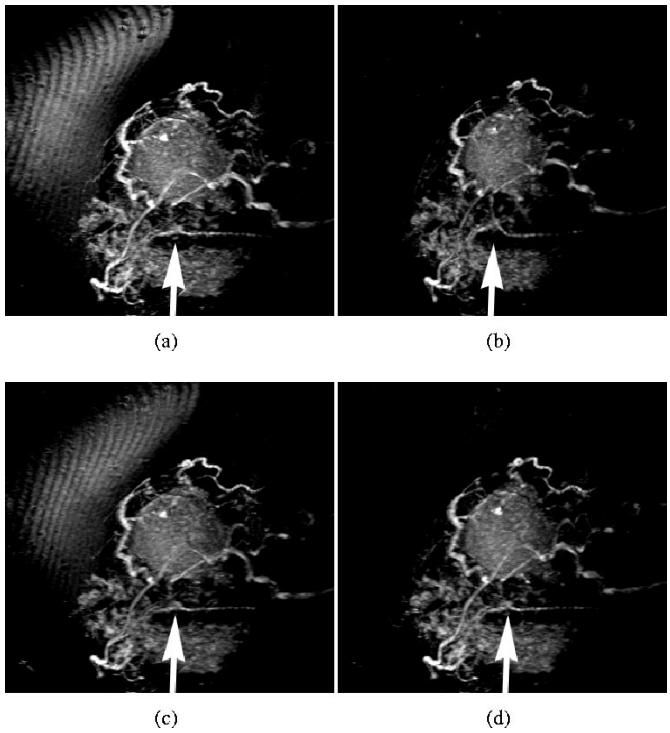

Fig. 12. Effect of alternating constraints on motion artifacts in maximum intensity projections of subtraction images. In two patients, there were substantial residual motion artifacts after volume-preserving nonrigid registration. The worse case is shown in this figure. (a) After rigid registration. (b) After unconstrained nonrigid registration (30% volume loss). (c) After nonrigid registration with incompressibility constraint (1% volume loss). (d) After nonrigid registration with alternating incompressibility constraint (1% volume loss). The unconstrained nonrigid registration reduces motion artifacts but shrinks the contrast enhancing lesion by 30% and also causes some change in the shape of structures, e.g., the arrow points to a bending that appears in a contrast-enhancing vessel after unconstrained registration. The incompressibility constraint with the normal search strategy preserves the lesion volume and the vessel morphology but does not in this case compensate for motion artifacts. The incompressibility constraint with alternating constraints optimization preserves the lesion volume and the vessel morphology and also substantially reduces motion artifacts.

of the identified lesion within 2%, substantially reduced the motion artifacts in all but one case, and the artifact reduction was "comparable with" (i.e., only slightly worse than) that of the unconstrained registration in 15 out of 17 cases. The worst case is shown in Fig. 12 and is discussed below. The smoothness constraint also substantially reduced the motion artifacts in all but one case, but the artifact reduction was comparable to that of the unconstrained registration in only 13 out of 17 cases.

We also note that, unlike the incompressibility constraint, the smoothness constraint in some cases causes increased volume loss of contrast-enhancing structures as compared with unconstrained registration. We suspect that this is the result of the smoothing effect the constraint has on the search space. Therefore, while the optimization may get stuck in a local minimum without the constraint, it can sometimes reach a better solution when the overall cost function is regularized. The incompressibility constraint, while it could potentially have a similar effect, does not cause increased volume loss, most likely because it inherently favors volume-preserving solutions.

In two patients of our study, there are substantial residual motion artifacts after volume-preserving nonrigid registration.

TABLE I
ALGORITHM PARAMETERS DURING MULTILEVEL NONRIGID REGISTRATION

Algorithm	Level	CPG Spacing	Voxel Size	Constraint Weight
Standard	1	40 mm	4 mm	ω
	2	20 mm	2 mm	ω
	3	10 mm	1 mm	ω
	4	5 mm	original	ω
Alternating Constraints	1	40 mm	4 mm	$10^{-2}\omega$
	2	40 mm	4 mm	ω
	3	20 mm	2 mm	$10^{-2}\omega$
	4	20 mm	2 mm	ω
	5	10 mm	1 mm	$10^{-2}\omega$
	6	10 mm	1 mm	ω
	7	5 mm	original	$10^{-2}\omega$
	8	5 mm	original	ω

The worst case is shown in Fig. 12. We believe that this is not always a consequence of constraining the free-form deformation, but is often an effect of the search algorithm used for optimization. At the cost of approximately doubled computation time, this problem can be addressed by using an alternating constraints search strategy recently introduced by us [34]. In addition to constraining the free-form deformation using a weighted penalty term, we also apply a scheme similar to simulated annealing. The idea is to first underconstrain the deformation, allowing the nonrigid registration to remove motion artifacts at the cost of shrinking contrast-enhancing structures. In a subsequent step, the deformation is then overconstrained, reexpanding the previously shrunk structures while deemphasizing the image similarity measure.[3] Table I lists the CPG spacing, voxel size, and constraint weight at each level of the hierarchical registration process.

The purpose of this search strategy is to help the registration process avoid local minima. This is particularly relevant for the incompressibility constraint, where the control points can get stuck in a local minimum in a situation somewhat analogous to the problem of mesh lock in finite element modeling. The search strategy alternately deforms the coordinate space based primarily on the image similarity measure (low-constraint weight) and then allows the space to relax (high-constraint weight). Underconstraining was achieved in the present study by multiplying the respective overconstraining weight by 10^{-2}.

We believe that it might be possible to achieve both goals of the nonrigid registration process, motion artifact reduction and lesion volume preservation, simultaneously using the alternating constraints search strategy (Table I). Results using this search strategy are illustrated for one patient in Fig. 12. Using only the incompressibility constraint with a sufficiently high weight to achieve volume preservation, not all motion artifact present after rigid registration [Fig. 12(a)] can be eliminated [Fig. 12(c)]. By alternating between lower and higher constraint weights at each level, virtually all motion artifact is removed with negligible volume loss using the incompressibility constraint [Fig. 12(d)], resulting in motion artifact reduction comparable to that achieved by unconstrained nonrigid registration [Fig. 12(b)]. The alternating constraints search strategy is promising, and we plan on further evaluating its usefulness in future work.

The validation of nonrigid registration algorithms is difficult and is an active area of research. In this study, we demonstrated that the use of an incompressibility penalty term can produce free-form deformations of MR breast images that substantially reduce motion artifact with negligible volume loss of contrast-enhancing structures. But, we did not show that the deformation fields are more accurate than those produced without using a penalty term. Schnabel *et al.* [39], [45] have recently reported promising results using a simulation of deformations based on biomechanical modeling of tissue properties to validate nonrigid registration methods. An important next step in this work is to evaluate the use of the incompressibility penalty term by using such a validation method.

[3]This idea is similar to the alternation of deformation and Gaussian smoothing as described in [49]. Note, however, that the "smoothing" step in our case is not a separate and purely mathematical operation as it is in [49], but instead is another deformation step with an increased weight on the regularization term.

ACKNOWLEDGMENT

All computations were performed on an SGI Origin 3800 supercomputer in the Stanford University Bio-X Core Facility for Biomedical Computation, Stanford, CA. The authors thank the anonymous reviewers for many helpful comments and suggestions.

REFERENCES

[1] Y. Amit, U. Grenander, and M. Piccioni, "Structural image restoration through deformable templates," *J. Amer. Statist. Assoc.*, vol. 86, pp. 376–387, 1991.
[2] R. Bajcsy and S. Kovacic, "Multiresolution elastic matching," *Comput. Vis.. Graph. Image Processing*, vol. 46, pp. 1–20, 1989.
[3] F. L. Bookstein, "Principal warps: Thin-plate splines and the decomposition of deformations," *IEEE Trans. Pattern Anal. Machine Intell.*, vol. 11, pp. 567–585, June 1989.
[4] P. Cachier and D. Rey, "Symmetrization of the nonrigid registration probem using inversion-invariant energies: Application to multiple sclerosis," in *Proc. Medical Image Computing and Computer-Assisted Intervention (MICCAI 2000)*, S. L. Delp, A. M. DiGioia, and B. Jaramaz, Eds., 2000, pp. 472–481.
[5] H. Chang and J. M. Fitzpatrick, "A technique for accurate magnetic resonance imaging in the presence of field inhomogeneities," *IEEE Trans. Med. Imag.*, vol. 11, pp. 319–329, Sept. 1992.
[6] G. E. Christensen, S. Joshi, and M. Miller, "Volumetric transformation of brain anatomy," *IEEE Trans. Med. Imag.*, vol. 16, pp. 864–877, Dec. 1997.
[7] G. E. Christensen and H. J. Johnson, "Consistent image registration," *IEEE Trans. Med. Imag.*, vol. 20, pp. 568–582, July 2001.
[8] G. E. Christensen, R. D. Rabbitt, and M. I. Miller, "Deformable templates using large deformation kinematics," *IEEE Trans. Image Processing*, vol. 5, pp. 1435–1447, Oct. 1996.
[9] A. Collignon, F. Maes, D. Delaere, D. Vandermeulen, P. Suetens, and G. Marchal, "Automated multimodality image registration using information theory," in *Proc. Information Processing in Medical Imaging (IPMI 1995)*, Y. Bizais, C. Barillot, and R. Di Paola, Eds., 1995, pp. 263–274.
[10] C. Davatzikos, "Spatial transformation and registration of brain images using elastically deformable models," *Comput. Vis. Image Understand.*, vol. 66, pp. 207–222, 1997.
[11] E. R. E. Denton, L. I. Sonoda, D. Rueckert, D. L. G. Hill, M. O. Leach, and D. J. Hawkes, "Comparison and evaluation of rigid, affine, and nonrigid registration of breast MR images," *J. Comput. Assist. Tomogr.*, vol. 23, pp. 800–805, 1999.
[12] P. J. Edwards, D. L. G. Hill, J. A. Little, and D. J. Hawkes, "A three-component deformation model for image-guided surgery," *Med. Image. Anal.*, vol. 2, pp. 355–367, 1998.

[13] J. M. Fitzpatrick, "The existence of geometrical density image transformations corresponding to object motion," *Comput. Vis. Graph. Image Processing*, vol. 44, pp. 155–174, 1988.

[14] J. M. Fitzpatrick, D. L. G. Hill, and C. R. Maurer Jr., *Handbook of Medical Imaging, Volume 2: Medical Image Processing and Analysis*, M. Sonka and J. M. Fitzpatrick, Eds. Bellingham, WA: SPIE, 2000, pp. 447–513. Image registration.

[15] D. R. Forsey and R. H. Bartels, "Hierarchical B-spline refinement," *Comput. Graph. (ACM)*, vol. 22, pp. 205–212, 1988.

[16] A. Hagemann, K. Rohr, H. S. Stiehl, U. Spetzger, and J. M. Gilsbach, "Biomechanical modeling of the human head for physically based, nonrigid image registration," *IEEE Trans. Med. Imag.*, vol. 18, pp. 875–884, Oct. 1999.

[17] J. V. Hajnal, D. L. G. Hill, and D. J. Hawkes, Eds., *Medical Image Registration*. Boca Raton, FL: CRC, 2001.

[18] T. Hartkens, D. L. G. Hill, C. R. Maurer Jr., A. J. Martin, W. A. Hall, D. J. Hawkes, D. Rueckert, and C. L. Truwit, "Quantifying the intraoperative brain deformation using interventional MR imaging," in *Proc. Int. Soc. Magn. Reson. Med.*, vol. 8, 2000, p. 51.

[19] P. Hayton, M. Brady, L. Tarassenko, and N. Moore, "Analysis of dynamic MR breast images using a model of contrast enhancement," *Med. Image. Anal.*, vol. 1, pp. 207–224, 1997.

[20] B. K. P. Horn and B. G. Schunck, "Determining optical flow," *Artif. Intell.*, vol. 17, pp. 185–203, 1981.

[21] S. Lee, G. Wolberg, and S. Y. Shin, "Scattered data interpolation with multilevel B-splines," *IEEE Trans. Visual. Comput. Graphics*, vol. 3, pp. 228–244, July-Sept. 1997.

[22] J. A. Little, D. L. G. Hill, and D. J. Hawkes, "Deformations incorporating rigid structures," *Comput. Vis. Image Understand.*, vol. 66, pp. 223–232, 1997.

[23] R. Lucht, M. V. Knopp, and G. Brix, "Elastic matching of dynamic MR mammographic images," *Magn. Reson. Med.*, vol. 43, pp. 9–16, 2000.

[24] V. R. Mandava, J. M. Fitzpatrick, and D. R. Pickens, "Adaptive search space scaling in digital image registration," *IEEE Trans. Med. Imag.*, vol. 8, pp. 251–262, Sept. 1989.

[25] C. R. Meyer, J. L. Boes, B. Kim, P. H. Bland, K. R. Zasadny, P. V. Kison, K. Koral, K. A. Frey, and R. L. Wahl, "Demonstration of accuracy and clinical versatility of mutual information for automatic multimodality image fusion using affine and thin-plate spline warped geometric deformations," *Med. Image. Anal.*, vol. 1, pp. 195–206, 1997.

[26] J. A. Nelder and R. Mead, "A simplex method for function minimization," *Comput. J.*, vol. 7, pp. 308–313, 1965.

[27] L. W. Nunes, M. D. Schnall, and S. G. Orel, "Update of breast MR imaging architectural interpretation model," *Radiology*, vol. 219, pp. 484–494, 2001.

[28] L. W. Nunes, M. D. Schnall, S. G. Orel, M. G. Hochman, C. P. Langlotz, C. A. Reynolds, and M. H. Torosian, "Breast MR imaging: Interpretation model," *Radiology*, vol. 202, pp. 833–841, 1997.

[29] W. H. Press, S. A. Teukolsky, W. T. Vetterling, and B. P. Flannery, *Numerical Recipes in C: The Art of Scientific Computing*, Cambridge, U.K.: Cambridge Univ. Press, 1988.

[30] R. M. Rangayyan, N. M. El-Faramawy, J. E. L. Desautels, and O. A. Alim, "Measures of acutance and shape for classification of breast tumors," *IEEE Trans. Med. Imag.*, vol. 16, pp. 799–810, Dec. 1997.

[31] A. Rappoport, A. Sheffer, and M. Bercovier, "Volume-preserving free-form solids," *IEEE Trans. Visual. Comput. Graphics*, vol. 2, pp. 19–27, Mar. 1996.

[32] T. Rohlfing and C. R. Maurer Jr., "Intensity-based nonrigid registration using adaptive multilevel free-form deformation with an incompressibility constraint," in *Proc. Medical Image Computing and Computer-Assisted Intervention (MICCAI 2001)*, W. Niessen and M. A. Viergever, Eds., 2001, pp. 111–119.

[33] ——, "Non-rigid image registration in shared-memory multiprocessor environments with application to brains, breasts, and bees," *IEEE Trans. Inform. Technol. Biomed.*, vol. 7, pp. 16–25, Mar. 2003.

[34] T. Rohlfing, C. R. Maurer Jr., M. A. Jacobs, D. A. Bluemke, and R. Shahidi, "An alternating-constraints algorithm for volume-preserving nonrigid registration of contrast-enhanced MR mammography images," in *Proc. Computer Assisted Radiology and Surgery (CARS 2002)*, H. U. Lemke, M. W. Vannier, K. Inamura, A. G. Farman, K. Doi, and J. H. C. Reiber, Eds., 2002, pp. 439–444.

[35] T. Rohlfing, C. R. Maurer Jr., W. G. O'Dell, and J. Zhong, "Modeling liver motion and deformation during the respiratory cycle using intensity-based free-form registration of gated MR images," *Proc. SPIE*, vol. 4319, pp. 337–348, 2001.

[36] D. Rueckert, "Nonrigid registration: Concepts, algorithms, and applications," in *Medical Image Registration*, J. V. Hajnal, D. L. G. Hill, and D. J. Hawkes, Eds. Boca Raton, FL: CRC, 2001, pp. 281–301.

[37] D. Rueckert, L. I. Sonoda, C. Hayes, D. L. G. Hill, M. O. Leach, and D. J. Hawkes, "Nonrigid registration using free-form deformations: Application to breast MR images," *IEEE Trans. Med. Imag.*, vol. 18, pp. 712–721, Aug. 1999.

[38] J. A. Schnabel, D. Rueckert, M. Quist, J. M. Blackall, A. D. Castellano-Smith, T. Hartkens, G. P. Penney, W. A. Hall, H. Liu, C. L. Truwit, F. A. Gerritsen, D. L. G. Hill, and D. J. Hawkes, "A generic framework for nonrigid registration based on nonuniform multi-level free-form deformations," in *Proc. Medical Image Computing and Computer-Assisted Intervention (MICCAI 2001)*, W. Niessen and M. A. Viergever, Eds., 2001, pp. 573–581.

[39] J. A. Schnabel, C. Tanner, A. D. Castellano Smith, M. O. Leach, C. Hayes, A. Degenhard, R. Hose, D. L. G. Hill, and D. J. Hawkes, "Validation of nonrigid registration using finite element methods," in *Proc. Information Processing in Medical Imaging (IPMI 2001)*, M. F. Insana and R. M. Leahy, Eds., 2001, pp. 344–357.

[40] T. W. Sederberg and S. R. Parry, "Free-form deformation and solid geometric models," *Comput. Graph. (ACM)*, vol. 20, pp. 151–160, 1986.

[41] C. Studholme, R. T. Constable, and J. S. Duncan, "Accurate alignment of functional EPI data to anatomical MRI using a physics-based distortion model," *IEEE Trans. Med. Imag.*, vol. 19, pp. 1115–1127, Nov. 2000.

[42] C. Studholme, D. L. G. Hill, and D. J. Hawkes, "Automated three-dimensional registration of magnetic resonance and positron emission tomography brain images by multiresolution optimization of voxel similarity measures," *Med. Phys.*, vol. 24, pp. 25–35, 1997.

[43] ——, "An overlap invariant entropy measure of 3D medical image alignment," *Pattern Recogn.*, vol. 32, pp. 71–86, 1999.

[44] C. Tanner, J. A. Schnabel, D. Chung, M. J. Clarkson, D. Rueckert, D. L. G. Hill, and D. J. Hawkes, "Volume and shape preservation of enhancing lesions when applying nonrigid registration to a time series of contrast enhancing MR breast images," in *Proc. Medical Image Computing and Computer-Assisted Intervention (MICCAI 2000)*, S. L. Delp, A. M. DiGioia, and B. Jaramaz, Eds., 2000, pp. 327–337.

[45] C. Tanner, A. Degenhard, J. A. Schnabel, A. D. Castellano Smith, C. Hayes, L. I. Sonoda, M. O. Leach, D. R. Hose, D. L. G. Hill, and D. J. Hawkes, "A method for the comparison of biomechanical breast models," in *Proc. IEEE Workshop Mathematical Methods in Biomedical Image Analysis (MMBIA 2001)*, L. Staib, Ed., 2001, pp. 11–18.

[46] D. Terzopoulos, "Regularization of inverse visual problems involving discontinuities," *IEEE Trans. Pattern Anal. Machine Intell.*, vol. PAMI-8, pp. 413–424, 1986.

[47] D. Terzopoulos and K. Waters, "Analysis and synthesis of facial image sequences using physical and anatomical models," *IEEE Trans. Pattern Anal. Machine Intell.*, vol. 16, pp. 569–579, June 1993.

[48] A. N. Thikhonov and V. Y. Arsenin, *Solutions of Ill-Posed Problems*. New York: Wiley, 1977.

[49] J.-P. Thirion, "Image matching as a diffusion process: An analogy with Maxwell's demons," *Med. Image. Anal.*, vol. 2, pp. 243–260, 1998.

[50] P. A. Viola, "Alignment by maximization of mutual information," Ph.D. dissertation, Massachusetts Inst. Technol., Cambridge, MA, 1995.

[51] G. Wahba, *Spline Models for Observational Data*. Philadelphia, PA: SIAM, 1990.

[52] J. B. West, J. M. Fitzpatrick, M. Y. Wang, B. M. Dawant, C. R. Maurer Jr., R. M. Kessler, R. J. Maciunas, C. Barillot, D. Lemoine, A. Collignon, F. Maes, P. Suetens, D. Vandermeulen, P. A. van den Elsen, S. Napel, T. S. Sumanaweera, B. Harkness, P. F. Hemler, D. L. G. Hill, D. J. Hawkes, C. Studholme, J. B. A. Maintz, M. A. Viergever, G. Malandain, X. Pennec, M. E. Noz, G. Q. Maguire Jr., M. Pollack, C. A. Pelizzari, R. A. Robb, D. Hanson, and R. P. Woods, "Comparison and evaluation of retrospective intermodality brain image registration techniques," *J. Comput. Assist. Tomogr.*, vol. 21, pp. 554–566, 1997.